scientific reports

Check for updates

OPEN

Towards site-specific information on PET degrading enzymes using NMR near operational temperature

Valeria Gabrielli[1], Jelena Grga[1], Sabine Gavalda[2], Laura Perrot[2], François-Xavier Cantrelle[3,4], Emmanuelle Boll[3,4], Guy Lippens[1]✉ & Cyril Charlier[1]✉

PETases are enzymes that can break down the poly-ethylene terephthalate (PET) polymer in its constituent building blocks. This enzymatic recycling process offers a sustainable solution for producing new, high-quality plastics from previously used materials. NMR spectroscopy can help in understanding and ultimately improving these enzymes but is always confronted with the lengthy step of acquisition and interpretation of triple resonance spectra for the spectral assignment. Here, we explore whether this step can be made more efficient by recording the spectra directly at high temperature, which simultaneously corresponds to more realistic working conditions for the enzyme. Taking the inactive variant of LCC^{ICCG} as an example, we compare spectral quality at 30°C and 50°C, and find that the latter condition greatly improves the Signal-to-Noise (S/N) ratio of the standard triple resonance spectra. Going up to 60°C, we show that pulse sequences mainly used for the assignment of intrinsically disordered proteins (IDPs) also become feasible. As a result, we present a methodology enabling exhaustive backbone assignment based on a minimal set of triple resonance spectra acquired and analysed in less than two weeks. The assignment process hence can be completed on a time scale comparable to crystallography, bringing NMR in a favourable position to contribute to bio-structural studies on this family of highly thermostable PETases.

Among analytical techniques, biomolecular Nuclear Magnetic Resonance (NMR) stands out as an exceptionally versatile approach for probing the structure, function and dynamics of biomolecules, with particular strength in enzyme characterization[1,2]. Nevertheless, recent advances in structural biology, including the rapid progress of cryo-electron microscopy (cryo-EM)[3], the continued improvements in X-ray crystallography[4,5] and the rise of powerful computational modelling have reshaped how researchers obtain structural insights into proteins[6]. This paradigm shift has, in turn, posed new challenges for biomolecular NMR spectroscopy, compelling the field to refine its identity and emphasize the unique advantages it offers[7,8]. Despite demanding initial stages, which often require specialized NMR facilities for tasks such as sample preparation (including stable isotope labeling), data acquisition through multiple triple- resonance experiments and complex data analysis like resonance assignment, biomolecular NMR provides an unparalleled ability to probe mechanistic details of enzymes at atomic level directly in solution[9]. In the past decades, important breakthroughs have continued to push the boundaries of what is achievable. Innovations include cell-free labeling systems[10], more efficient data acquisition (Non-Uniform Sampling[11], SO-FAST[12]), automated resonance assignment procedures[13–15] and integrative approaches that combine NMR with artificial intelligence (AI) to address long-standing challenges[16,17]. Contemporary NMR spectroscopy clearly needs to take the best of these advances to open up to new horizons.

In the field of biotechnology, enzyme optimization is for many programs the key towards the success of bio-based approaches[18]. Computational methods based on artificial intelligence[19,20] thereby can generate huge libraries of potential candidates, and coupled to high-throughput screening methods[21], have the potential to rapidly converge upon improved enzymes. If NMR spectroscopy wants to participate in this effort – and convince that its site-specific information is most useful for example to restrict the list of potential mutation sites for directed evolution[9,22], obtaining a fully assigned ^{1}H-^{15}N spectrum as rapidly as possible seems a strict requirement.

One recent example where enzymes are at the core of a promising industrial process is bio-enzymatic recycling of plastic[23]. PET hydrolases (PETases) break the ester linkages in polyethylene terephthalate (PET), a common

[1]Toulouse Biotechnology Institute (TBI), University of Toulouse, CNRS, INRAE, INSA Toulouse, 135 Avenue de Rangueil, 31077 Toulouse Cedex 04, France. [2]Carbios, Parc Cataroux–Bâtiment B80, 8 rue de la Grolière, 63100 Clermont-Ferrand, France. [3]CNRS EMR 9002—Integrative Structural Biology, 59000 Lille, France. [4]Univ. Lille, Inserm, CHU Lille, Institut Pasteur de Lille UMR 1167—RID-AGE—Risk Factors and Molecular Determinants of Aging-Related Diseases, 59000 Lille, France. ✉email: glippens@insa-toulouse.fr; charlier@insa-toulouse.fr

plastic used in the manufacturing of beverage bottles, food containers or clothing fibers. In this rapidly evolving field, many newly identified PETase enzymes from diversity[24] have been screened and used as starting points for further engineering. It proved essential to work close to the PET glass temperature of ~ 70°C, where the plastic becomes more dynamic at the molecular level without yet crystallizing[25]. The temperature of denaturation of the enzymes thereby has become an important factor next to their intrinsic catalytical efficacy. The initially mesophilic *Ideonella sakaiensis* (*Is*) PETase[26] with its T_m of 46.1°C was evolved to become the ThermoPETase (Tm 58.6°C; Son et al.[27]), FastPETase (Tm 56.9°C; Lu et al.[28]), DepoPETase (Tm 69.4°C; Shi et al.[29]), DuraPETase (Tm 78.7°C; Cui et al.[30]) and finally HotPETase (Tm 82.5°C; Bell et al.[31]). Derived from the thermophilic Leaf-branch Compost Cutinase (LCC)[32], a thermostable cutinase characteristic from the type I group[33], its quadruple mutant LCC^{ICCG} was equally optimized based on its activity as well as its thermostability (T_m = 85.8°C for LCC and 93.3°C for LCC^{ICCG} at pH 8, both proteins without C-terminal His-tag)[23]. The latter enzyme has shown great promise for industrial application of plastic recycling[34,35].

From an NMR standpoint, this high thermostability could be - at least in theory- a significant advantage, as spectral recording at higher temperatures should lead to faster tumbling of the enzyme and hence mimic a lower molecular weight species. Here, taking the catalytically inactive S165A variant of LCC^{ICCG} as an example, we explore the possibility to facilitate the resonance assignment of the thermophilic PETases by recording a set of 3D experiments directly at higher temperatures. We first measure experimentally the global tumbling time (τ_c) at different temperatures, and find a twofold reduction already when going from 30°C to 50°C. When comparing spectra at 30°C, temperature where we obtained our first assignments[36], and similar experiments recorded at 50°C, we find that the standard triple resonance experiments work significantly better at 50°C, with an important gain in Signal-to-Noise (S/N) ratio and hence reduction in spectral recording time. We equally find that additional experiments based on the hNcaNNH and HncaNNH pulse sequences[37], mostly used for assignment of highly flexible Intrinsically Disordered Proteins (IDPs) although equally applied with success to some larger enzymes after complete deuteration[38,39], become feasible without any deuteration, and this despite the 30 kDa MW range of the enzymes. Based on this observation, we achieve *de novo* backbone assignment of an active variant of LCC^{ICCG} primarily based on the resulting ^{15}N and $^{1}H^{N}$ connectivities. Within 6 days of data acquisition followed by 3 days of data analysis, nearly 75% of the $^{15}N/^{1}H^{N}$ resonances were assigned. Such achievement should enable NMR to follow protein design at a pace at least comparable to X-ray crystallography and alleviate the bottleneck of resonance assignment in large scale projects involving thermostable enzymes.

Materials and methods

Protein expression and purification

LCC^{ICCG}-S165A and its active variant were expressed and purified according to previous studies[36,40].

NMR spectroscopy

LCC^{ICCG}-S165A

All experiments recorded for backbone assignment at 50°C were acquired on a 800 MHz spectrometer equipped with a 5-mm cryoprobe with pulsed field z-gradients. The sample contained 580 µM of ^{15}N-^{13}C labeled protein in 25 mM Tris-HCl buffer pH 7.5 with 100 mM NaCl. The data presented here were recorded using the standard Bruker library pulse sequences: 2D ^{1}H-^{15}N HSQC, HNCACB and HNCO. All spectra were processed using Topspin 4.0.8 (Bruker Biospin). Spectral analysis for backbone assignments was performed manually using POKY[41]. One important experimental factor we found when measuring at higher temperatures is the necessity to seal the sample. Otherwise, already after a day, evaporation set in and shim quality rapidly deteriorated. Spectral dimensions for the HNCO experiments were 3622 Hz (F_1) × 2919 Hz (F_2) × 12500 Hz (F_3) corresponding to 18 × 36 × 15.6224 ppm, with sampling durations of 15.5 ms (t_1), 10.9 ms (t_2), 160 ms (t_3). Spectra were centered at 4.7 ppm (^{1}H), 117.5 ppm (^{15}N), 173 ppm (^{13}CO). Spectral settings for the HNCACB experiment were 6438.5 Hz (F_1) × 2919 Hz (F_2) × 14084.25 Hz (F_2) corresponding to 32 × 36 × 50 ppm, with sampling durations of 14.9 ms (t_1), 10.9 ms (t_2), 0.009 ms (t_3). Spectra were centered at 4.7 ppm (^{1}H), 117.5 ppm (^{15}N), 40 ppm ($^{13}C\alpha$). Both experiments were acquired with 4 scans per increment.

Active variant of LCC^{ICCG}

Experiments were recorded at 60 °C on a sample containing 600 µM of ^{15}N-^{13}C labeled of the active variant of LCC^{ICCG} in 25 mM Tris-HCl buffer pH 7.5 with 100 mM NaCl on a 900 MHz spectrometer equipped with a 5-mm cryoprobe with pulsed field z-gradients with the parameters shown in Table 1:

NUS percentages were estimated based on the number of resonances expected in each dataset. Data were reconstructed using standard MDD software[42]. Spectral analysis and backbone assignments were performed manually using CcpNmr analysis software v2.5[43].

TRACT analysis

TRACT spectra were recorded with the pulse sequence of Lee et al., implemented as individual experiments for the α and β ^{15}N spin states[44]. A relaxation delay of 3 s was used between scans, and 4k points were recorded. A total of 24 delays ranging from 1 to 200 ms were sampled as increments in a pseudo-2D matrix and recorded with 512 scans per delay. After manual phasing and baseline correction, the integral of the [10.0-6.4] ppm region was determined and plotted as a function of the corresponding delay. The resulting curve was fitted as a mono-exponentially decaying function, and the difference between the rates of both components was interpreted in terms of τ_c as described by Robson et al.[45].

Theoretical calculus of the τ_c value as a function of temperature was performed by fixing the τ_c value at the experimentally determined value of 13 ns for 30°C, and then applying the following formula[46] :

	Time domain data size (points)			Spectral width/carrier frequency (ppm)		
	t1	t2	t3	F1 (^{1}H)	F2(^{15}N)	F3
^{1}H,^{15}N HSQC	3076	128		19.83/4.7	35/117	
HNCACB	4000	128	128	15.42/4.7	35/117	60/42 (^{13}C)
HNCO	4000	128	112	15.42/4.7	35/117	13/173.5 (^{13}C)
HNcaCO	4000	128	112	15.42/4.7	35/117	13/173.5 (^{13}C)
hNcaNNH	2048	128	128	13.88/4.7	35/117	35/117 (^{15}N)
HncaNNH	4000	128	512	15.42/4.7	35/117	6/8 (^{1}H)
	NS	Delay time (s)	NUS (%)	Pulse program	Exp time	
^{1}H,^{15}N HSQC	4	1	–	hsqcf3gpph19	9 min 55 s	
HNCACB	16	1	25	hncacbgpwg3d	22 h 54 min	
HNCO	4	1	8	hncogpwg3d	1 h 35 min	
HNcaCO	16	1	15	hncacogpwg3d	12 h 5 min	
hNcaNNH	64	1	13	hncannhgp3d	1 d 22 h 46 min	
HncaNNH	64	1	3.6	hncannhgp3d.2	2 d 6 h 48 min	

Table 1. List of experiments used for the assignment of the active variant of LCC^{ICCG}.

$$\tau_c(30\,^{\circ}C) = \frac{\eta_{30\,^{\circ}C}}{\eta_T} * \frac{273+T}{303} * \tau_c(T)$$

where η_T is the viscosity of water at the temperature T (using the Celsius scale). The latter was calculated using the equation from[47]

$$\eta_T = 1.7753 - 0.0565T + 1.0751 * 10^{-3}T^2 - 9.222 * 10^{-6}T^3$$

.

or, alternatively, from[48]:

$$log(\eta_T/\eta_{20}) = \frac{(20-T)}{(T+96)} \times 1.2378 - 1.303 * 10^{-3}(20-T) + 3.06 * 10^{-6}(20-T)^2 + 2.55 * 10^{-8}(20-T)^3$$

and does not consider that our protein sample was not in pure water but rather in 25mM Tris-HCl and 100mM NaCl buffer pH 7.5.

Results

Determination of τ_c as function of temperature

The global tumbling time τ_c (or, strictly speaking, the correlation time of the dipolar autocorrelation function of a given amide H-N vector[49]) is one criterium that determines the linewidth of the corresponding amide correlation peak. Other factors such as chemical exchange of the amide protons with water or the presence of dynamics in the intermediate time scale regime can equally contribute. Whereas the ratio of transverse (T_2) to longitudinal (T_1) relaxation times can be used to estimate this τ_c parameter[50], the increasing influence of intramolecular motions on the T_1 relaxation time for larger proteins[51] has motivated the development of an alternative method. The TRACT (TRosy for rotAtional Correlation Times) method measures the decay of both TROSY and anti-TROSY components of the ^{15}N doublet[44], and translates the differential rate into a value of τ_c without interference of dipole–dipole (DD) relaxation by remote protons or relaxation contributions from chemical exchange[44,45]. TRACT experiments on the LCC^{ICCG}-S165A enzyme were recorded at various temperatures ranging from 30°C to 60°C. By integrating the envelope of the proton spectra over the amide region as a function of the relaxation delay, both (TROSY and anti-TROSY) relaxation rates were obtained using an exponential minimization (Fig. 1. A & B). The difference between both rates (ΔR_2) was interpreted using the equation given by Robson and coauthors[45] and yielded τ_c values varying from 13 to 5.7 ns upon increasing the temperature from 30°C to 60°C (Fig. 1. C). The reduction of τ_c is expected, and follows well the temperature dependence of water viscosity expected for a rigid body of this size[46] (Fig. 1.D). The small discrepancy at higher temperature could come for the buffer and salt concentrations influencing the viscosity[52]. Importantly, accelerated tumbling predicts a significant decrease in transverse relaxation rates for both amide and Cα resonances[53], thereby reducing the need for (partial) deuteration of the sample. We show here that because of this superior sensitivity, nearly complete assignment of the backbone and side chain spectra of LCC^{ICCG}-S165A can be obtained with a minimal set of experiments recorded at 50°C (Mathematical details are given in in the methods section).

Influence of the temperature on spectral quality

To evaluate experimentally the influence of temperature on the spectral quality of our PETase, we recorded on the same sample at 30°C and 50°C both the ^{1}H-^{15}N HSQC and ^{1}H-^{15}N TROSY correlation spectra using standard Bruker pulse programs (*hsqcf3gpph19* and *trosyf3gpph19*). Already at 30°C, signal intensity improved

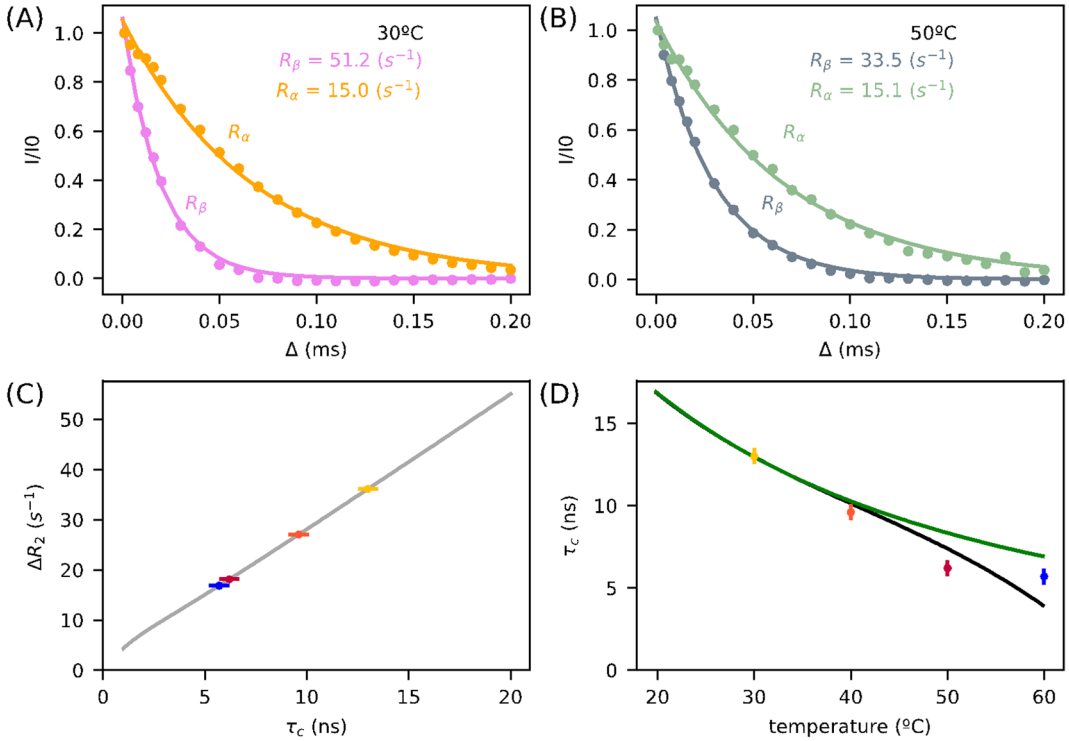

Fig. 1. Determination of the correlation time τ_c as function of temperature. (**A**,**B**) TRACT analysis of LCC^{ICCG}-S165A at (**A**) 30°C and (**B**) 50°C. Both panels display the single-spin-state ^{15}N R_α and $R_\beta$relaxation decay curves obtained using the TRACT sequence. The dots represent the experimental points, and the lines represent the results of fitting the curves to a single exponential decay. (**C**) Theoretical curve of the difference between ^{15}N relaxation rates, ΔR_2 as function of τ_c following the equations of Robson and coworkers[45]. (**D**) Theoretical curve of the temperature dependence of τ_c as predicted for a protein with its τ_c at 30°C fixed at 13 ns, based on the temperature dependence of water viscosity. Solid lines shows the τ_c values as a function of temperature as calculated with water viscosity according to Weast[47] (black) or Kestin et al.[48] (green). On **C** and **D** panels, dots correspond to experimental values at 30°C (yellow), 40°C (orange), 50°C (red) and 60°C (blue). Error bars on (**C**) and (**D**) were calculated based on and estimated uncertainty of +/- 0.5 s^{-1} for the fits of the R_α and R_β curves.

by ~ 40% when comparing the HSQC experiment with the TROSY version, and going to 50°C clearly boosted the intensity gain by another ~ 15% (Fig. 2.A). Equally important, the number of peaks in the 2D correlation spectra remained nearly the same between spectra recorded at both temperatures (Fig. 2.B), indicating limited solvent exchange.

Further time-saving could be obtained by BEST-[54] or SOFAST-[12] HSQC sequences and should therefore be considered before setting up any triple resonance experiment. However, the reduced spin-diffusion at higher temperatures should diminish the difference between selective and non-selective relaxation after excitation of the amide proton pool, which is the underlying principle of these pulse sequences[36]. Moreover, due to the presence of extreme ^1H chemical shifts for some amide protons of LCC^{ICCG} (reaching 10.9 ppm or 5.6 ppm), the use of these schemes in our particular case led to the loss of ~ 10 resonances (Figure S1), and was therefore not pursued in the present study. In accordance with the lower τ_c value, NOE based magnetization transfer proved slower at 50°C than at 30°C[55], but should simultaneously suffer less from spin diffusion (Figure S2).

In a typical backbone assignment experiment (e.g. HNCACB), the lengthy back-transfer of $^{13}C\alpha$ to ^{15}N magnetization is often a limiting step due to the rapid relaxation of the $^{13}C\alpha$ transverse magnetization. While in a HMQC experiment, this loss is amplified by the short ^1H transverse relaxation time, the HSQC experiment is less impacted as the ^1H magnetization is stored along the z-axis and the ^1H T_1 is long . This is exemplified when comparing ^1H-^{13}C HMQC and HSQC at 30°C where one can clearly see the increased number of visible resonances in the HSQC experiment (Figure S3). To evaluate how beneficial spectral recording at 50°C would be, we then measured ^{1H}-^{13}CHSQC spectra with a wide ^{13}C spectral window both at 30°C and 50°C (Fig. 2.C). Relative to the isolated methyl signal of M166[56], we observe a nearly 40% increase in intensity for $^1H\alpha$-$^{13}C\alpha$ resonances in the spectrum recorded at 50°C compared to that at 30°C. To evaluate the effect this has on triple resonance spectra, we acquired a series of ^1H-^{13}C planes from HNCO, HNcaCO and HNCACB spectra using the Bruker standard HSQC-based (*hncogpwg3d*, *hncacogpwg3d*, *hncacbgpwg3d*) experiments both at 30 °C and 50°C. When comparing the ^1H spectra resulting from the 1st Free Induction Decay (FID) for HNCO and HNcaCO and the positive sum of the HNCACB plane we observe significant improvement in the S/N ratio of 20–30% for HNCO and 50% for HNcaCO and HNCACB when measuring at 50°C (Fig. 2D and Figure S4). This

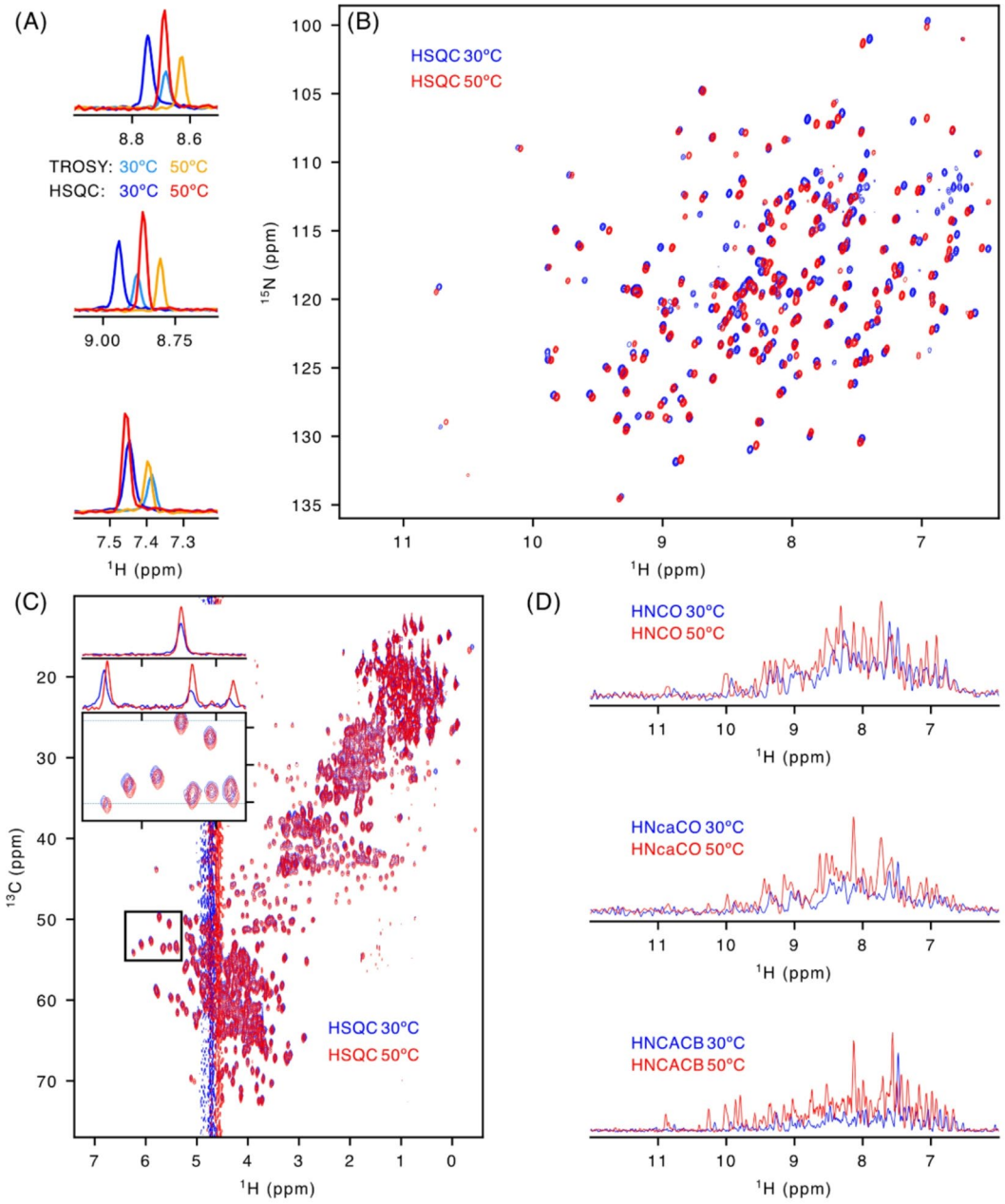

Fig. 2. Selection of the best conditions and experiments for PETase assignment LCC^{ICCG}-S165A. (**A**) 1D ^{1}H slices through G88 (top), A59 (middle), G163 (bottom) cross peaks from ^{1}H-^{15}N HSQC at 30°C (blue), ^{1}H-^{15}N TROSY at 30°C (light-blue), ^{1}H-^{15}N HSQC at 50°C (red) and ^{1}H-^{15}N TROSY at 50°C (orange). (**B**) ^{1}H-^{15}N HSQC at 30°C (blue) and 50°C (red). Cross peaks generally shift upfield, but their number is the same at both temperatures (**C**) ^{1}H-^{13}C HSQC at 30°C (blue) and 50°C (red). The insets show how representative ^{13}Cα signals are sharper at 50°C compared to 30°C. The ^{1}H 1D slices were taken at the ^{13}C frequency displayed by the dashed lines. (**D**) 1D plot of the 1st FID of HNCO (top) and HNcaCO (middle) along with a positive projection of a HNCACB experiment (bottom) measured at 30°C (blue) and 50°C (red).

improvement can be confirmed by the results of an automatic peak detection performed on the respective planes, that finds for both HNcaCO and HNCACB planes nearly twice the number of resonances at 50°C compared to identical dataset at 30°C. A detailed analysis of the increase of observable peaks is presented in the SI.

To obtain the resonance assignment of LCC^{ICCG}-S165A, we recorded a full HSQC-based HNCACB triple resonance spectrum at 50 °C and pH 7.5. Starting from our previous assignment of the ^{1}H-^{15}N HSQC spectrum of LCC^{ICCG}-S165A at 30°C[56] which at the time required nearly 4 weeks of experimental time, we used this single spectrum to confirm the assignments at 50°C (Figure S5). A HNCO experiment was recorded to obtain the ^{13}C' resonances at 50°C. In total, 85% of the ^{1}H^{N}/^{15}N resonances along with 91% for ^{13}Cα (234 out of 258), 90% ^{13}Cβ

(215 out of 239 residues, excluding the 19 glycines) and 85% of $^{13}C'$ resonances (203 out of 239, excluding all residues preceding a proline residue) were assigned.

Raising the temperature for hNcaNNH

In our general effort to accelerate the assignment of the ^{1}H-^{15}N spectrum, we explored the possibility to record a hNcaNNH experiment[37]. While the common approach of backbone assignment consists of connecting consecutive residues through their various ^{13}C resonances, these experiments have been developed to obtain sequential correlations between successive amide proton and nitrogen resonances $^{1}H_{(i-1)}$, $^{15}N_{(i-1)}$, $^{1}H_{(i)}$, $^{15}N_{(i)}$, $^{1}H_{(i+1)}$, $^{15}N_{(i+1)}$[37,57,58]. Although recognized as true game changers in the assignment process for disordered proteins[59,60], they have not been used for non-deuterated globular proteins of the size of PETases due to their inherent low sensitivity. Indeed, the bottleneck in these experiments is the fast ^{13}Ca relaxation rate that significantly deteriorates their sensitivity. To explore whether these experiments would profit from the same sensitivity gain as the above-described triple resonance spectra with a single period of ^{13}Ca transverse relaxation, we recorded a hNcaNNH at 30°C and 50°C with the standard pulse sequence from the Bruker library (hncannhgp3d).

At 30 °C, no signal could be observed (Figure S6), and when raising the temperature to 50 °C the sensitivity of this experiment proved at the edge ($S/N < 5$ for most peaks) in a reasonable amount of experimental time (2 days 15 hours for a fully sampled dataset) (Fig. 3.A). However, the signal-to-noise ratio further increased by an average 70%, and even by a factor of two for certain residues (Figure S7) when raising the temperature to 60°C (Fig. 3.A). For many resonances where the connecting peaks were absent in the spectrum at 50°C, we obtained at 60°C the connection through their $^{15}N_{(i-1)}$ and $^{15}N_{(i+1)}$ resonances. (Fig. 3.B).

Rapid de novo backbone assignment

Based on the quality of the hNcaNNH acquired at 60°C, we sought to investigate whether a *de novo* backbone assignment primarily based on the hNcaNNH and HncaNNH experiments would be possible. Turning stretches of connecting resonances into a backbone assignment further required a HNCACB spectrum to obtain amino acid type identifying ^{13}C chemical shift values (Fig. 4). Finally, we recorded HNCO and HNcaCO spectra for independent verification of the obtained assignments (Table 1). With a 500 µM sample of the active enzyme in a 5 mm tube, on a 900 MHz spectrometer equipped with a triple-resonance cryogenically cooled probe head, the complete data set was acquired within 6 days of machine time (see Methods).

The elevated temperature (60°C) led to improved signal-to-noise data and further allowed efficient non-uniform sampling providing very high-resolution spectra. Especially for the HncaNNH experiment, this enhanced resolution proved important to establish firm $^{1}H^{N}$ connectivities between resonances of neighboring residues and thereby to speed up significantly the assignment procedure. To complement the assignment strategy, the HNCACB experiment was employed to confirm the sequential connectivity of residues. This experiment enables the identification of both intra-residue (i) and preceding residue (i-1) carbon (Cα and Cβ) resonances, thereby establishing the directionality of the assignments.

As the overall goal of our work was to streamline and accelerate the backbone resonance assignment of thermostable enzymes, we tested NMRtist, an AI-driven tool that enables automated processing from peak picking to resonance assignment and ultimately to structure calculation[14]. NMRtist requires as input the amino acid sequence of the target protein together with peak lists derived from 2D and 3D NMR spectra. Accordingly, we prepared peak lists of ^{1}H-^{15}N-HSQC and 3D HNCO, HNcoCA, HNCACB, HncaNNH, and hNcaNNH spectra. Automated peak-picking was performed with CCP-NMR v2 software, since NMRtist does not currently

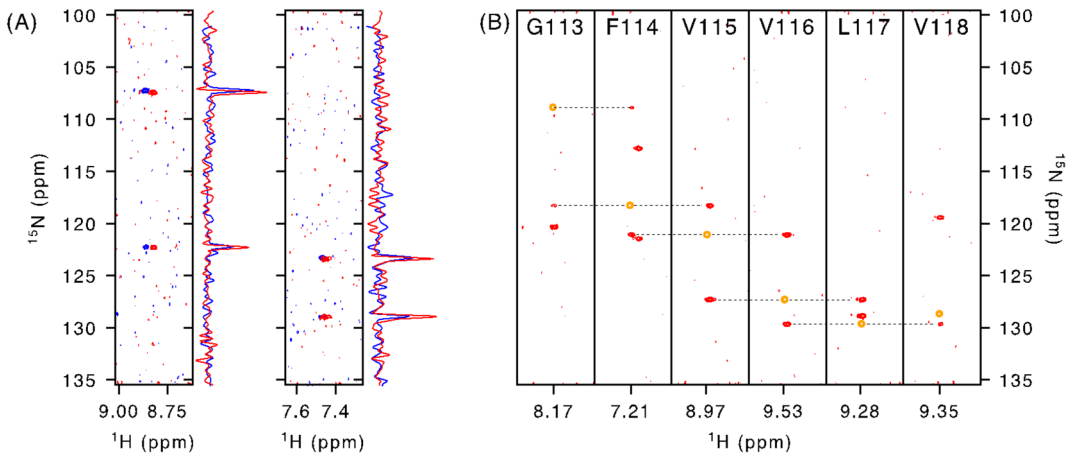

Fig. 3. Connecting ^{15}N resonances through hNcaNNH experiment. (**A**) Overlay of the ^{1}H-^{15}N strip extracted from the hNcaNNH at 50°C (blue) and 60°C (red) for A59 and L203. ^{15}N traces were extracted at the ^{1}H frequency of the selected signal. (**B**) ^{1}H-^{15}N strips of consecutive residues at 60°C shown for residues from G113 to V118. Red resonances correspond to $^{15}N(i-1)$ and $^{15}N(i+1)$ while the autocorrelation cross-peak leading to the $^{15}N(i)$ was added manually in orange based on the ^{15}N value obtained from the ^{1}H-^{15}N HSQC spectra.

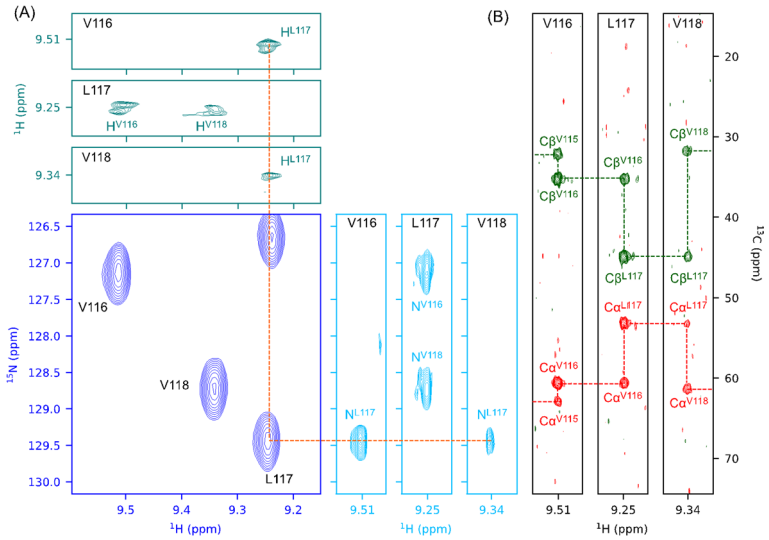

Fig. 4. De novo assignment primarily based on ^{15}N and ^{1}H connectivities. (**A**) Example of connectivity between the HncaNNH (teal), HSQC (blue) and hNcaNNH (skyblue) experiments for residues V116-L117-V118. The ^{1}H-^{1}H and ^{15}H-^{1}H strips were extracted at the $^1H^N$ resonance frequency of the 3 signals. The strips are only displayed in the window corresponding to the HSQC experiment (blue). The resonances of V115 and I119 respectively on the V116 and V118 strips are outside of displayed window. The orange line shows the connectivity for L117 both from V116 (i-1) and L118 (i + 1). (**B**) HNCACB strips displayed for all 3 residues with the Cα in red and Cβ in green.

support peak picking for HncaNNH and hNcaNNH spectra. When providing only the carbon-connectivity-based spectra (HNCO, HNcoCA, HNCACB) along ^{1}H-^{15}N-HSQC peak lists, NMRtist returned an estimated chemical shift assignment coverage of 46%. This value increased to 65% upon inclusion of the HncaNNH and hNcaNNH peak lists as input. The inclusion of HncaNNH and hNcaNNH peak lists hence significantly improves the overall assignment score, despite the fact that these spectra are underrepresented in the training data, potentially leading to reduced performance. Therefore, we proceeded simultaneously with a manual backbone resonance assignment. Within three days of spectral analysis, and without relying on the previously generated NMRtist outputs, we successfully assigned nearly 80% of backbone (^{1}H/^{15}N) resonances (Figure S8). A comparison between the manual and NMRtist-derived assignments revealed inaccuracies in the latter which are likely attributable to the fact that our PETase, with its 258 amino acids, lies at the upper limit of the protein size range for which NMRtist was trained. In addition, the slightly lower percentage than the one obtained previously for the inactive LCC^{ICCG} variant is primarily due to additional broadening of some resonances assigned to solvent exposed residues that were already at the limit of observation at 50 °C in LCC^{ICCG}-S165A (T211 and G127; see Figure S5).

Discussion

The initial steps of the development of new or improved PETases have invariably involved molecular modeling and/or bioinformatics, whereby the starting 3D structures that served as input for these efforts mostly came from X-ray crystallography. Examples such as *Tf*Cut2 (PDB code: 4CG1[61]), Cut190 (5ZNO[62]), LCC and mutants (4EBO[32] and 6THS, 6THT[34]) or *Is*PETase (5XG0[63]), are reviewed by Liu et al.[64] and Tournier et al.[23].

Solution biomolecular NMR has only recently entered this field, and not as much as to obtain structural information but to characterize the interaction between the enzyme and small soluble substrates[56,65] or to investigate the role of the catalytic histidine with its associated pKa value[40]. Recently, a solid state NMR study of the *Tf*Cut2 enzyme embedded in a trehalose glass in the presence of nanoparticles (NPs) made of ^{13}C labeled PET oligomers equally added to our understanding of the enzyme/polymer interaction and the biocatalytic mechanism of the hydrolase reaction[66]. However, if NMR wants to consolidate its place in this large-scale project that is the development of industrial PETases, easy, rapid and robust methods providing the assignment of the ^{1}H-^{15}N and/or ^{1}H-^{13}C spectra are required.

Our study demonstrates that recording NMR experiments at elevated temperatures can significantly accelerate backbone resonance assignment of thermostable PETases. Using the TRACT approach[44,45], we observed that the overall global tumbling time was reduced by approximately a factor of two, effectively making a 25 kDa protein behave like a ~ 10 kDa protein in the NMR tube. Furthermore, the sensitivity increase that accompanies the line narrowing by this apparent molecular weight decrease (Fig. 2) is not counteracted by opposing effects such as increased exchange with the water or other line broadening effects. Indeed, we observed very limited amide proton exchange up to 50°C/60°C, with only a couple of resonances less intense compared to 30°C. This sharply contrasts with the case of IDPs where amide proton signals at neutral to alkaline pH completely disappear at higher temperatures[67,68]. An upfield shift for most of the amide protons is observed at the high temperature, due to weakened hydrogen bonding[69–71]. It is not clear at this moment whether the pH dependence of our Tris buffer

at higher temperature (with a predicted lowering of 0.3 units between 30°C and 50°C) contributes to this shift or to limiting the water exchange. Finally, NOE build-up curves at both temperatures (Figure S2) showed the feasibility of recording a high-resolution NOESY-HSQC spectrum even at 50 °C, and could thereby provide the experimental data for efforts to assign the ^{1}H-^{15}N HSQC on the sole basis of a 3D NOESY-HSQC experiment together with the experimental (or predicted) 3D structure[14,72].

Particularly true for enzymes near or beyond 30 kDa, considered the size-limit of classical solution state NMR, assignment of the ^{1}H-^{15}N HSQC spectrum remains a real bottleneck for many projects in which NMR is or could be involved. Except for intrinsically disordered proteins (IDPs), where the relevant τ_c parameter does not correlate with the MW of the protein, the size problem leads not only to an increased number of peaks but also to peak broadening and hence decreased signal-to-noise. Deuteration[73–75] together with TROSY approaches[36] can alleviate the latter peak broadening, but significantly increases the price per sample, with associated costs that become an important factor to consider in a program that generates many variants. Altogether, we observe in the Biomagresbank[76] an exponentially decreasing number of deposited assignments for proteins larger than 150 residues, and finally no more than ~ 100 entries for proteins of the size of LCC and its derivatives[14].

Although the NMR assignment clearly will never keep up with the many PETase variants that are currently tested in academic and industrial laboratories all over the world, speeding up the process could increase its use in this rapidly evolving field. Not only do we increase the sensitivity of the standard triple resonance experiments that are the cornerstone of the assignment process by matching ^{13}C frequencies (Fig. 2.D), but directly connecting consecutive amide peaks through the complementary hNcaNNH or HncaNNH spectra becomes possible (Figs. 3 and 4) and dramatically speeds up the procedure, be it manual or (semi-)automatic. High temperatures equally imply we are studying these enzymes in what we would call 'near-working industrial conditions"[35] (to make the parallel with "near-physiological conditions" for disease related enzymes), and should therefore be seen as a win-win situation for solution state NMR : it not only yields higher-quality data and opens the door to experiments that would otherwise be impossible, but it also gives information about the enzyme in conditions that approximate its real-world functioning.

Data availability

All the parameter sets for the NMR spectra have been deposited to https://zenodo.org/records/15425383 and/or contact either glippens@insa-toulouse.fr or charlier@insa-toulouse.fr. Chemical shifts have been deposited on BMRB under the number 53331.

Received: 16 May 2025; Accepted: 29 September 2025
Published online: 04 November 2025

References

1. East, K. W. et al. NMR and computational methods for molecular resolution of allosteric pathways in enzyme complexes. *Biophys. Rev.* **12**, 155–174 (2020).
2. Shein, M. et al. Characterizing ATP processing by the AAA + protein p97 at the atomic level. *Nat. Chem.* **16**, 363–372 (2024).
3. Chua, E. Y. D. et al. Better, faster, cheaper: recent advances in cryo–electron microscopy. *Annu. Rev. Biochem.* **91**, 1–32 (2022).
4. Liu, H. & Lee, W. The XFEL protein crystallography: developments and perspectives. *IJMS* **20**, 3421 (2019).
5. Mous, S., Poitevin, F., Hunter, M. S., Asthagiri, D. N. & Beck, T. L. Structural biology in the age of X-ray free-electron lasers and exascale computing. *Curr. Opin. Struct. Biol.* **86**, 102808 (2024).
6. Rosignoli, S., Pacelli, M., Manganiello, F. & Paiardini, A. An outlook on structural biology after A Lpha F old: tools, limits and perspectives. *FEBS Open. Bio.* **15**, 202–222 (2025).
7. Karamanos, T. K. & Matthews, S. Biomolecular NMR in the AI-assisted structural biology era: old tricks and new opportunities. *Biochim. Et Biophys. Acta (BBA) - Proteins Proteom.* **1872**, 140949 (2024).
8. Selenko, P. Quo vadis biomolecular NMR spectroscopy? *IJMS* **20**, 1278 (2019).
9. Bhattacharya, S. et al. NMR-guided directed evolution. *Nature* **610**, 389–393 (2022).
10. Hoffmann, B., Löhr, F., Laguerre, A., Bernhard, F. & Dötsch, V. Protein labeling strategies for liquid-state NMR spectroscopy using cell-free synthesis. *Progress Nucl. Magn. Reson. Spectrosc.* **105**, 1–22 (2018).
11. Hoch, J. C., Maciejewski, M. W., Mobli, M., Schuyler, A. D. & Stern, A. S. In *Encyclopedia of Magnetic Resonance* (ed. Harris, R. K.) emrstm1239 https://doi.org/10.1002/9780470034590.emrstm1239 (John Wiley & Sons, Ltd, 2012).
12. Schanda, P., Kupče, Ē. & Brutscher, B. SOFAST-HMQC experiments for recording two-dimensional deteronuclear correlation spectra of proteins within a few seconds. *J. Biomol. NMR.* **33**, 199–211 (2005).
13. Bishop, A. C., Torres-Montalvo, G., Kotaru, S., Mimun, K. & Wand, A. J. Robust automated backbone triple resonance NMR assignments of proteins using Bayesian-based simulated annealing. *Nat. Commun.* **14**, 1556 (2023).
14. Klukowski, P., Riek, R. & Güntert, P. Time-optimized protein NMR assignment with an integrative deep learning approach using alphafold and chemical shift prediction. *Sci. Adv.* **9**, eadi9323 (2023).
15. Pritišanac, I., Würz, J. M., Alderson, T. R. & Güntert, P. Automatic structure-based NMR methyl resonance assignment in large proteins. *Nat. Commun.* **10**, 4922 (2019).
16. Rasulov, U. et al. Protein NMR assignment by isotope pattern recognition. *Sci. Adv.* **10**, eado0403 (2024).
17. Shukla, V. K., Heller, G. T. & Hansen, D. F. Biomolecular NMR spectroscopy in the era of artificial intelligence. *Structure* **31**, 1360–1374 (2023).
18. Katsimpouras, C. & Stephanopoulos, G. Enzymes in biotechnology: critical platform technologies for bioprocess development. *Curr. Opin. Biotechnol.* **69**, 91–102 (2021).
19. Reisenbauer, J. C., Sicinski, K. M. & Arnold, F. H. Catalyzing the future: recent advances in chemical synthesis using enzymes. *Curr. Opin. Chem. Biol.* **83**, 102536 (2024) https://doi.org/10.1016/j.cbpa.2024.102536.
20. Yang, J., Li, F. Z. & Arnold, F. H. Opportunities and challenges for machine learning-assisted enzyme engineering. *ACS Cent. Sci.* **10**, 226–241 (2024).
21. Yew, M., Yang, Y., Wang, Q. & Zhu, L. High-throughput screening strategies for plastic-depolymerizing enzymes. *Trends Biotechnol.* S0167779924003871 https://doi.org/10.1016/j.tibtech.2024.12.008 (2025).
22. Gutierrez-Rus, L. I. et al. Enzyme enhancement through computational stability design targeting NMR-determined catalytic hotspots. *Preprint at.* https://doi.org/10.26434/chemrxiv-2024-7xxzg (2024).
23. Tournier, V. et al. Enzymes' power for plastics degradation. *Chem. Rev.* **123**, 5612–5701. https://doi.org/10.1021/acs.chemrev.2c00644 (2023).

24. Lin, X. et al. Natural-selected plastics biodegradation species and enzymes in landfills. *PNAS Nexus*. **4**, pgaf066 (2025).
25. Thomsen, T. B., Hunt, C. J. & Meyer, A. S. Influence of substrate crystallinity and glass transition temperature on enzymatic degradation of polyethylene terephthalate (PET). *New Biotechnol.* **69**, 28–35 (2022).
26. Yoshida, S. et al. A bacterium that degrades and assimilates poly(ethylene terephthalate). *Science* **351**, 1196–1199 (2016).
27. Son, H. F. et al. Rational protein engineering of thermo-stable PETase from *Ideonella sakaiensis* for highly efficient PET degradation. *ACS Catal.* **9**, 3519–3526 (2019).
28. Lu, H. et al. Machine learning-aided engineering of hydrolases for PET depolymerization. *Nature* **604**, 662–667 (2022).
29. Shi, L. et al. Complete depolymerization of PET wastes by an evolved PET hydrolase from directed evolution. *Angew Chem. Int. Ed.* **62**, e202218390 (2023).
30. Cui, Y. et al. Computational redesign of a PETase for plastic biodegradation under ambient condition by the GRAPE strategy. *ACS Catal.* **11**, 1340–1350 (2021).
31. Bell, E. L. et al. Directed evolution of an efficient and thermostable PET depolymerase. *Nat. Catal.* **5**, 673–681 (2022).
32. Sulaiman, S. et al. Isolation of a novel cutinase homolog with polyethylene terephthalate-degrading activity from leaf-branch compost by using a metagenomic approach. *Appl. Environ. Microbiol.* **78**, 1556–1562 (2012).
33. Joo, S. et al. Structural insight into molecular mechanism of poly(ethylene terephthalate) degradation. *Nat. Commun.* **9**, 382 (2018).
34. Tournier, V. et al. An engineered PET depolymerase to break down and recycle plastic bottles. *Nature* **580**, 216–219 (2020).
35. Arnal, G. et al. Assessment of four engineered PET degrading enzymes considering Large-Scale industrial applications. *ACS Catal.* 13156–13166. https://doi.org/10.1021/acscatal.3c02922 (2023).
36. Pervushin, K., Riek, R., Wider, G. & Wüthrich, K. Attenuated T 2 relaxation by mutual cancellation of dipole–dipole coupling and chemical shift anisotropy indicates an avenue to NMR structures of very large biological macromolecules in solution. *Proc. Natl. Acad. Sci. U S A*. **94**, 12366–12371. https://doi.org/10.1016/j.bpj.2022.07.002 (1997).
37. Weisemann, R., Rüterjans, H. & Bermel, W. 3D Triple-resonance NMR techniques for the sequential assignment of NH and 15 N resonances in 15 N- and 13 C-labelled proteins. *J. Biomol. NMR* **3**, (1993).
38. Frueh, D. P. et al. Non-uniformly sampled double-TROSY hNcaNH experiments for NMR sequential assignments of large proteins. *J. Am. Chem. Soc.* **128**, 5757–5763 (2006).
39. Frueh, D. P. Practical aspects of NMR signal assignment in larger and challenging proteins. *Progress Nucl. Magn. Reson. Spectrosc.* **78**, 47–75 (2014).
40. Charlier, C. et al. Exploring the pH dependence of an improved PETase. *Biophys. J.* S0006349524002881 https://doi.org/10.1016/j.bpj.2024.04.026 (2024).
41. Lee, W., Rahimi, M., Lee, Y. & Chiu, A. POKY: a software suite for multidimensional NMR and 3D structure calculation of biomolecules. *Bioinformatics* **37**, 3041–3042 (2021).
42. Mayzel, M., Kazimierczuk, K. & Orekhov, V. Y. The causality principle in the reconstruction of sparse NMR spectra. *Chem. Commun.* **50**, 8947–8950 (2014).
43. Vranken, W. F. et al. The CCPN data model for NMR spectroscopy: development of a software pipeline. *Proteins* **59**, 687–696 (2005).
44. Lee, D., Hilty, C., Wider, G. & Wüthrich, K. Effective rotational correlation times of proteins from NMR relaxation interference. *J. Magn. Reson.* **178**, 72–76 (2006).
45. Robson, S. A., Dağ, Ç., Wu, H. & Ziarek, J. J. TRACT revisited: an algebraic solution for determining overall rotational correlation times from cross-correlated relaxation rates. *J. Biomol. NMR*. **75**, 293–302 (2021).
46. De La García, J., Huertas, M. L. & Carrasco, B. H. Y. D. R. O. N. M. R. Prediction of NMR relaxation of globular proteins from atomic-level structures and hydrodynamic calculations. *J. Magn. Reson.* **147**, 138–146 (2000).
47. *CRC Handbook of Chemistry and Physics. A Ready-Reference Book of Chemical and Physical Data*. (CRC P, 1979).
48. Kestin, J., Sokolov, M. & Wakeham, W. A. Viscosity of liquid water in the range – 8°C to 150°C. *J. Phys. Chem. Ref. Data*. **7**, 941–948 (1978).
49. Cavanagh, J., Fairbrother, W. J., Palmer, A. G., Rance, M. & Skeltonv, N. J. In *Protein NMR Spectroscopy (Second Edition)* (eds Cavanagh, J. et al.) v–vi https://doi.org/10.1016/B978-012164491-8/50000-2 (Academic Press, 2007).
50. Tjandra, N., Feller, S. E., Pastor, R. W. & Bax, A. Rotational diffusion anisotropy of human ubiquitin from 15 N NMR relaxation. *J. Am. Chem. Soc.* **117**, 12562–12566 (1995).
51. Luginbühl, P. Semi-classical nuclear spin relaxation theory revisited for use with biological macromolecules. *Progress Nucl. Magn. Reson. Spectrosc.* **40**, 199–247 (2002).
52. Woldeyes, M. A., Qi, W., Razinkov, V. I., Furst, E. M. & Roberts, C. J. How well do low- and high-concentration protein interactions predict solution viscosities of monoclonal antibodies? *J. Pharm. Sci.* **108**, 142–154 (2019).
53. Yamazaki, T., Lee, W., Arrowsmith, C. H., Muhandiram, D. R. & Kay, L. E. A suite of triple resonance NMR experiments for the backbone assignment of 15 N, 13 C, 2H labeled proteins with high sensitivity. *J. Am. Chem. Soc.* **116**, 11655–11666 (1994).
54. Schanda, P., Van Melckebeke, H. & Brutscher, B. Speeding up three-dimensional protein NMR experiments to a few minutes. *J. Am. Chem. Soc.* **128**, 9042–9043 (2006).
55. Neuhaus, D. & Williamson, M. P. *The Nuclear Overhauser Effect in Structural and Conformational Analysis* (Wiley, 2000).
56. Charlier, C. et al. An NMR look at an engineered PET depolymerase. *Biophys. J.* **121**, 2882–2894 (2022).
57. Bracken, C., Iii, A. G. P. & Cavanagh, J. H)N(COCA)NH and HN(COCA)NH experiments for 1H-15 N backbone assignments in 13 C/15 N-labeled proteins. *J. Biomol. NMR.* **9**, 94–100 (1997).
58. Sun, Z. Y. J., Frueh, D. P., Selenko, P., Hoch, J. C. & Wagner, G. Fast assignment of 15 N-HSQC peaks using high-resolution 3D HNcocaNH experiments with non-uniform sampling. *J. Biomol. NMR.* **33**, 43–50 (2005).
59. Lopez, J., Ahuja, P., Gerard, M., Wieruszeski, J. M. & Lippens, G. A new strategy for sequential assignment of intrinsically unstructured proteins based on 15 N single isotope labelling. *J. Magn. Reson.* **236**, 1–6 (2013).
60. Charlier, C. et al. Structure and dynamics of an intrinsically disordered protein region that partially folds upon binding by chemical-exchange NMR. *J. Am. Chem. Soc.* **139**, 12219–12227 (2017).
61. Roth, C. et al. Structural and functional studies on a thermostable polyethylene terephthalate degrading hydrolase from thermobifida fusca. *Appl. Microbiol. Biotechnol.* **98**, 7815–7823 (2014).
62. Numoto, N. et al. Structural dynamics of the PET-degrading cutinase-like enzyme from *Saccharomonospora viridis* AHK190 in substrate-bound states elucidates the Ca^{2+}-driven catalytic cycle. *Biochemistry* **57**, 5289–5300 (2018).
63. Han, X. et al. Structural insight into catalytic mechanism of PET hydrolase. *Nat. Commun.* **8**, 2106 (2017).
64. Liu, F. et al. Current advances in the structural biology and molecular engineering of PETase. *Front. Bioeng. Biotechnol.* **11**, 1263996 (2023).
65. Hellesnes, K. N., Vijayaraj, S., Fojan, P., Petersen, E. & Courtade, G. Biochemical characterization and NMR study of a PET-hydrolyzing cutinase from *Fusarium Solani Pisi*. *Biochemistry* **62**, 1369–1375 (2023).
66. Falkenstein, P. et al. On the binding mode and molecular mechanism of enzymatic polyethylene terephthalate degradation. *ACS Catal.* **13**, 6919–6933 (2023).
67. Gil, S. et al. NMR spectroscopic studies of intrinsically disordered proteins at near-physiological conditions. *Angew Chem. Int. Ed.* **52**, 11808–11812 (2013).

68. Lopez, J., Schneider, R., Cantrelle, F., Huvent, I. & Lippens, G. Studying intrinsically disordered proteins under true in vivo conditions by combined cross-polarization and carbonyl-detection NMR spectroscopyy. *Angew Chem. Int. Ed.* **55**, 7418–7422 (2016).
69. Wagner, G. & Wüthrich, K. Structural interpretation of the amide proton exchange in the basic pancreatic trypsin inhibitor and related proteins. *J. Mol. Biol.* **134**, 75–94 (1979).
70. Baxter, N. J. & Williamson, M. P. Temperature dependence of 1H chemical shifts in proteins. *J. Biomol. NMR.* **9**, 359–369 (1997).
71. Asakura, T., Taoka, K., Demura, M. & Williamson, M. P. The relationship between amide proton chemical shifts and secondary structure in proteins. *J. Biomol. NMR.* **6** (1995).
72. Stratmann, D., Van Heijenoort, C. & Guittet, E. NOE *net*–use of NOE networks for NMR resonance assignment of proteins with known 3D structure. *Bioinformatics* **25**, 474–481 (2009).
73. Gardner, K. H. & Kay, L. E. The use of ^{2}H, ^{13}C, ^{15}N multidimensional NMR GTO study the structure and dynamics of proteins. *Annu. Rev. Biophys. Biomol. Struct.* **27**, 357–406 (1998).
74. LeMaster, D. M. & Richards, F. M. NMR sequential assignment of Escherichia coli thioredoxin utilizing random fractional deuteriation. *Biochemistry* **27**, 142–150 (1988).
75. Sattler, M. & Fesik, S. W. Use of deuterium labeling in NMR: overcoming a sizeable problem. *Structure* **4**, 1245–1249 (1996).
76. Hoch, J. C. et al. Biological magnetic resonance data bank. *Nucleic Acids Res.* **51**, D368–D376 (2023).

Acknowledgements

We would like to thank Alain Marty, Vincent Tournier and Nicolas Chabot (Carbios, France) for insightful discussions and comments on the manuscript. We thank the ICEO facility of the Toulouse Biotechnology Institute (TBI), which is part of the Integrated Screening Platform of Toulouse (PICT, IBiSA), for providing access to protein-purification equipment. We thank Dr. E. Cahoreau and L. Peyriga in the MetaToul (Toulouse metabolomics & fluxomics facilities, www.metatoul.fr) NMR facility. MetaToul is part of the French National Infrastructure for Metabolomics and Fluxomics MetaboHUB-AR-11-INBS-0010 (www.metabohub.fr), and is supported by the Région Midi-Pyrénées, the ERDF, the SICOVAL and the French Minister of Education & Research, who are all gratefully acknowledged. Financial support from the IR INFRANALYTICS FR2054 for conducting the research is gratefully acknowledged. This study was supported by the OPTIZYME grant financed by ADEME - contract number 2282D0513-C.

Author contributions

V.G., E.B. and F.-X.C. recorded and analysed NMR spectra. J.G., L.P. and S.G. resources. G.L. and C.C. conceptualization, project administration, supervision, writing – original draft preparation, writing - review & editing. All authors reviewed the manuscript.

Declarations

Competing interests

The authors declare no competing interests.

Additional information

Supplementary Information The online version contains supplementary material available at https://doi.org/10.1038/s41598-025-22351-1.

Correspondence and requests for materials should be addressed to G.L. or C.C.